

Mission: Impossible (Escape from the Lyman Limit) ^{*}

A. Fernández-Soto,^{1,2,†‡} K.M. Lanzetta,³ H.-W. Chen,^{4,5,§}

¹ *Osservatorio Astronomico di Brera, Via Bianchi 46, Merate (LC), I-23807, Italy*

² *Observatori Astronòmic, Universitat de València, Burjassot (València), E-46100, Spain*

³ *Department of Physics and Astronomy, State University of New York at Stony Brook, Stony Brook, NY 11794-3800, U.S.A.*

⁴ *The Observatories of the Carnegie Institution of Washington, 813 Santa Barbara Street, Pasadena, CA 91101, U.S.A.*

⁵ *Center for Space Research, Massachusetts Institute of Technology, Cambridge, MA 02139-4307, U.S.A.*

Accepted —. Received —; in original form —

ABSTRACT

We investigate the intrinsic opacity of high-redshift galaxies to outgoing ionising photons using high-quality photometry of a sample of 27 spectroscopically-identified galaxies of redshift $1.9 < z < 3.5$ in the Hubble Deep Field. Our measurement is based on maximum-likelihood fitting of model galaxy spectral energy distributions—including the effects of intrinsic Lyman-limit absorption and random realizations of intervening Lyman-series and Lyman-limit absorption—to photometry of galaxies from space- and ground-based broad-band images. Our method provides several important advantages over the methods used by previous groups, including most importantly that two-dimensional sky subtraction of faint-galaxy images is more robust than one-dimensional sky subtraction of faint-galaxy spectra. We find at the 3σ statistical confidence level that *on average* no more than 4% of the ionising photons escape galaxies of redshift $1.9 < z < 3.5$. This result is consistent with observations of low- and moderate-redshift galaxies but is in direct contradiction to a recent result based on medium-resolution spectroscopy of high-redshift ($z \approx 3$) galaxies. Dividing our sample in subsamples according to luminosity, intrinsic ultraviolet colour, and redshift, we find no evidence for selection effects that could explain such discrepancy. Even when all systematic effects are included, the data could not realistically accommodate any escape fraction value larger than $\approx 15\%$.

Key words: galaxies: formation — cosmology: observations — cosmology: diffuse radiations

1 INTRODUCTION

The diffuse ultraviolet background is one of the key ingredients in the recipe leading to galaxy formation (Miralda-Escudé & Ostriker 1990; Giroux & Shapiro 1996). The intensity of the diffuse ultraviolet background has been estimated at moderate and high redshifts using the proximity effect on QSO absorbers (Liske & Williger 2001; Scott *et al.* 2001; Fernández-Soto *et al.* 1995; Kulkarni & Fall 1993), and results obtained so far suggest that it is too large to be explained by QSOs alone (Madau & Shull 1996, but see also e.g. Giallongo *et al.* 1996). Although systematic errors may make these measurements uncertain (Loeb & Eisenstein 1995, Pascarella *et al.* 2001), several suggestions have

been put forward to explain the observed extra intensity. One of the most popular suggestions calls for the escape of a large fraction of ionising photons from high-redshift galaxies. If correct, this would imply that the interstellar media of high-redshift galaxies must be at least partially transparent to ionising photons.

But the best measurements available at low and moderate redshifts show that galaxies are (at least nearly) opaque to ionising photons. The large column densities of neutral hydrogen that surround most galaxies should be enough, depending on how they are distributed, to very effectively quench any outgoing flux of ionising photons. In fact, Leitherer *et al.* (1995) find, in a sample of four starburst galaxies at an average redshift $\langle z \rangle \approx 0.02$, that the limits to the escape fraction of Lyman limit photons range from $f_{\text{esc}} < 0.0095$ to $f_{\text{esc}} < 0.15$ (with an observed flux ratio at 900 Å and 1500 Å of $F_{9/15} < 0.10 - 0.20$). Hurwitz *et al.* (1997) analyse the same data and obtain slightly less stringent limits, ranging from $f_{\text{esc}} < 0.032$ to $f_{\text{esc}} < 0.57$. Deharveng *et al.* (2001) find a more stringent limit $f_{\text{esc}} < 0.064$

^{*} Based on observations taken with the NASA/ESA Hubble Space Telescope, which is operated by AURA under NASA contract NAS5-26555

[†] Marie Curie Fellow

[‡] Email: alberto.fernandez@uv.es

[§] Hubble Fellow

for a starburst galaxy of redshift $z = 0.0448$. At higher redshifts ($z \approx 1$), Ferguson (2001) finds similar upper limits $f_{\text{esc}} < 0.20$ to the escape fraction.

It is much less clear whether galaxies at still higher redshifts are as opaque to ionising photons as galaxies at low and moderate redshifts. Accurate measurements become progressively more difficult at higher redshifts, because galaxies are much fainter and the presence of Lyman α forest absorption introduces further uncertainties. The only two measurements available so far are from Steidel, Pettini & Adelberger (2001) and Giallongo *et al.* (2002). Adopting a correction factor for intervening Lyman α absorption determined from a composite QSO spectrum, Steidel *et al.* reported $F_{9/15} = 0.22 \pm 0.05$ using 29 galaxies at $\langle z \rangle = 3.40$, while Giallongo *et al.* reported a 1σ upper limit $F_{9/15} \lesssim 0.05$ using two galaxies at $z \sim 3$. The former measurement indicates that galaxies at $z \sim 3$ are much more transparent to ionising photons, contributing an equal amount of ionising flux to the ultraviolet background radiation as the QSOs. The latter measurement indicates otherwise.

In this article, we present a new measurement of f_{esc} using 27 galaxies at redshifts $1.9 < z < 3.5$ in the Hubble Deep Field (HDF). All of these galaxies have secure spectroscopic redshifts (see Cohen *et al.* 2000–C00 and Dawson *et al.* 2001–D01) and accurate broad-band photometry from HST/WFPC2 observations in the F300W, F450W, F606W, and F814W bandpasses. Our measurement is based on deep space-based images, which provides two important advantages over the methods used by previous groups: First, our sky subtraction is more accurate, because two-dimensional sky subtraction in faint-galaxy images is more robust than one-dimensional sky subtraction in faint-galaxy spectra. Second, the wavelength interval below the rest-frame Lyman limit over which we integrate is larger, because the space-based broad-band images are sensitive to observed-frame wavelengths as short as $\lambda \approx 2800 \text{ \AA}$, allowing us to integrate over rest-frame wavelength intervals as large as $\approx 100 \text{ \AA}$ in some cases. Our method also improves upon previous work by accounting for the effect of the Lyman α forest absorption by performing a large number of random realizations of a parameterized distribution, to account for variations of the absorbing clouds across different lines of sight.

Our results show that the escape fraction estimated from the ensemble of 27 galaxies has a (statistical) 3σ upper limit of $f_{\text{esc}} \lesssim 0.04$. Given that our galaxy sample spans a range of properties in redshift, intrinsic colours, and luminosities, we also explore possible systematic effects by dividing the galaxies into different subsamples. We do not find any evidence to support that bluer galaxies have higher escape fractions of ionizing photons. Instead, we find that more luminous galaxies appear to have shallower ultraviolet spectral slopes and higher escape fractions (at the 2σ level of significance). We do also search for other possible systematic effects that could be inherent to our method, and find that other effects cannot in any realistic way account for a large increase in the escape fraction.

2 DATA

We consider all galaxies in the HDF with known spectroscopic redshifts in the range $1.9 < z < 3.5$. The lower limit

Table 1. Properties of the galaxy sample used in the analysis. Celestial coordinates are J2000.

RA-12 ^h	Dec-62 ^o	FLY99	z	AB(814)
36:49.83	14:15.0	1016	1.980	23.40
36:48.32	14:16.6	1044	2.005	23.40
37:00.09	12:25.2	0048	2.050	23.77
36:54.73	13:14.8	0670	2.232	24.29
36:55.07	13:47.1	0831	2.233	24.52
36:50.11	14:01.1	0960	2.237	24.58
36:54.62	13:41.3	0806	2.419	25.27
36:45.88	14:12.1	1054	2.427	25.21
36:43.27	12:38.9	0664	2.442	24.81
36:53.19	13:22.7	0742	2.489	24.83
36:44.64	12:27.4	0517	2.500	23.73
36:41.72	12:38.8	0702	2.591	24.60
36:45.35	11:52.7	0175	2.799	23.24
36:44.09	13:10.8	0815	2.929	24.03
36:47.77	12:55.7	0687	2.931	23.95
36:46.93	12:26.1	0444	2.969	25.24
36:48.29	11:45.9	0021	2.980	25.07
36:53.43	13:29.4	0762	2.991	24.60
36:45.36	13:47.0	0964	3.160	25.09
36:51.20	13:48.8	0897	3.162	25.22
36:53.60	14:10.2	0955	3.181	24.55
36:41.23	12:02.9	0390	3.220	24.03
36:49.81	12:48.8	0568	3.233	25.18
36:52.99	14:08.5	0957	3.367	26.85
36:52.75	13:39.1	0825	3.369	25.07
36:52.41	13:37.8	0824	3.430	24.79
36:39.57	12:30.5	0688	3.475	25.40

is chosen so that the rest-frame Lyman limit begins to affect the photometry in the F300W bandpass. The upper limit is chosen so that we can still reasonably distinguish absorption due to the Lyman α forest from the intrinsic Lyman limit absorption. We previously measured high-quality photometry of these galaxies using HST/WFPC2 through the F300W, F450W, F606W, and F814W filters (Fernández-Soto, Lanzetta & Yahil 1999–FLY99 hereafter; Lanzetta *et al.* in preparation). The sample includes 27 galaxies, as given in Table 1. The reader is referred to FLY99, C00, D01, and Fernández-Soto *et al.* 2001 for more details on individual galaxies.

We determine the absolute AB magnitude of each galaxy using a fiducial spectral energy distribution determined from a template fitting technique that we will describe in the next section. We adopt a cosmological model with vacuum energy density $\Omega_{\Lambda} = 0.65$, matter density $\Omega_M = 0.35$, and a Hubble constant $H_0 = 65 \text{ km s}^{-1} \text{ Mpc}^{-1}$. Absolute AB magnitudes of the galaxies at rest-frame wavelengths $\lambda = 1500 \text{ \AA}$ range from ≈ -21.8 to ≈ -25.4 . Apart from these absolute magnitudes, all other results in this paper are independent of the chosen cosmological model.

3 METHOD

Our method is based on maximum-likelihood fitting of model galaxy spectral energy distributions, including the effects of intrinsic Lyman-limit absorption and random realizations of intervening Lyman-series and Lyman-limit ab-

sorption, to space- and ground-based broad-band images. In practice, our method proceeds in several steps as follows:

First, we determine a fiducial spectral energy distribution of each galaxy by fitting model spectral energy distributions to the broad-band photometric measurements that fall between rest-frame wavelengths $\lambda = 1250$ and 2800 \AA . The wavelength range is chosen to avoid the spectral discontinuity produced by the Lyman series (rest-frame wavelength $\lambda < 1215 \text{ \AA}$) and the Balmer break (rest-frame wavelengths $\lambda \gtrsim 3000 \text{ \AA}$). The fiducial spectral energy distributions are based on the six spectrophotometric templates (of E, Sbc, Scd, Irr, SB1, and SB2 galaxies) of our previous photometric redshift measurements (Yahata *et al.* 2000; see also Benítez 2000) together with a power-law form $f_\nu \propto \lambda^\alpha$. (The power-law form is required because a few of the galaxies are found to be bluer—in the ultraviolet rest-frame—than any of the starburst spectrophotometric templates. In each of these cases, $\alpha < 0.5$.) The spectral energy distributions are selected according to a χ^2 analysis similar to the analysis used for our previous photometric redshift measurements (Lanzetta *et al.* 1996; FLY99).

Next, we modify the fiducial spectral energy distribution of each galaxy by adding the effect of intrinsic Lyman-limit absorption, which is characterized by an assumed Lyman-limit optical depth τ_g that is taken to be universal across all galaxies. For a Lyman-limit optical depth τ_g , the output spectrum $f(\lambda, \tau_g)$ in terms of the input spectrum $f(\lambda, 0)$ at rest-frame wavelength λ is

$$f(\lambda, \tau_g) = f(\lambda, 0) \exp[-\tau_g(\lambda/\lambda_{LL})^3] \quad (1)$$

at rest-frame wavelengths $\lambda < \lambda_{LL}$, where λ_{LL} is the rest-frame wavelength of the Lyman limit.

Next, we modify the fiducial spectral energy distribution of each galaxy by adding the effect of random realizations of intervening Lyman series and Lyman limit absorption. Here we characterize the distribution of Lyman α forest absorption systems by a distribution function $F(N, b, z)$, which is defined in such a way that $F(N, b, z) dN db dz$ is the expected number of absorption systems in the neutral hydrogen column density interval dN around N , Doppler parameter interval db around b , and redshift interval dz around z . We adopt as the functional form of the distribution function

$$F(N, b, z) \propto (1+z)^\gamma N^{-\beta} G^*(\hat{b}, \sigma_b, b_{\min}), \quad (2)$$

where $G^*(\hat{b}, \sigma_b, b_{\min})$ is a “truncated” Gaussian distribution of mean \hat{b} , dispersion σ_b , and minimum truncation value b_{\min} . We adopt $\gamma = 2.5$, $\beta = 1.6$, $\hat{b} = 23 \text{ km s}^{-1}$, $\sigma_b = 8 \text{ km s}^{-1}$, and $b_{\min} = 15 \text{ km s}^{-1}$.

We have extensively checked that simulated spectra generated according to these parameters reproduce to within observed scatter the average Lyman α absorption D_A and average Lyman series absorption D_B . In Figure 1 we show the average values of D_A and D_B , compared to values found in the literature. The agreement is perfect within the scatter present in the observational data.

The incidence of Lyman limit systems (those with hydrogen opacity $\tau > 1$) is an important factor in our simulation, as they are amongst the main drivers of the absorption bluewards of the galactic Lyman edge. We plot in Figure 2 the density of Lyman limit systems generated by our Lyman α forest model, and compare it with the numbers measured

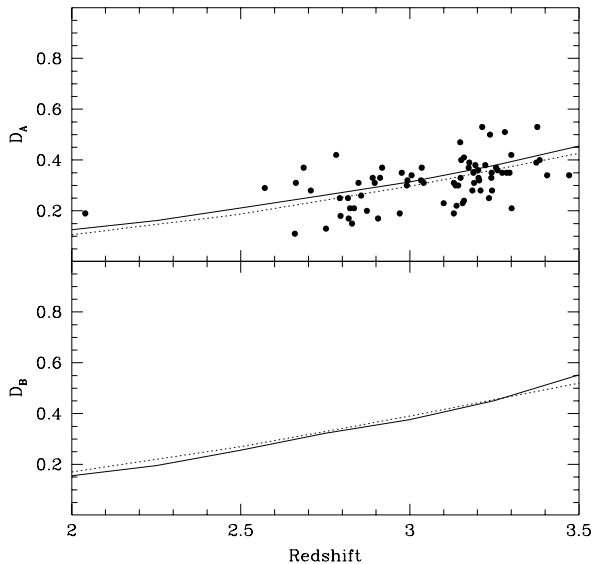


Figure 1. Values of the Lyman decrements D_A and D_B obtained by averaging 1000 spectra generated by our model at each redshift (continuous line). The curves are compared with the values by Webb (unpublished, dotted line) which our group uses for photometric redshift estimation, and with a compilation of D_A values obtained from the literature (Oke & Korycansky 1982; Bechtold *et al.* 1984; Steidel & Sargent 1987; O’Brian, Wilson & Gondhalekar 1988; Schneider, Schmidt, & Gunn 1989; Giallongo & Cristiani 1990; Schneider, Schmidt, & Gunn 1991).

by different authors (as described in the Figure). As can be seen, our model produces slightly less Lyman limit systems at the lowest redshifts than have been observed. Whereas this effect could produce a bias favouring lower escape fraction values, we have checked that this effect is not important (see SS4.2 and 4.3 for details). This slight defect is the result of our decision to adopt a single parameterization to generate all of the Lyman α forest—a change in the normalization to improve the aspect of Figure 2 would conflict with the data shown in Figure 1. Globally, we consider that our model reproduces within reasonable limits the properties of the intergalactic medium.

Next, we measure the simulated spectrum of each galaxy—constructed from the fiducial spectral energy distribution of each galaxy modified by the effects of intrinsic Lyman-limit absorption with an assumed Lyman-limit optical depth τ_g and of random realizations of intervening Lyman series and Lyman limit absorption—at short-wavelengths, i.e. over the F300W bandpass which is sensitive at wavelengths below the rest-frame Lyman limit, and we compare observed energy fluxes $f_{\text{obs}}^{(i)}$ and uncertainties $\sigma_{\text{obs}}^{(i)}$ and simulated energy fluxes $f_{\text{sim}}^{(i,j)}$ of the i th galaxy in the j th simulation. To randomize the effects of intervening Lyman series and Lyman limit absorption, we repeat this procedure a large number of times, and we form the likelihood as a function of Lyman-limit optical depth τ_g as

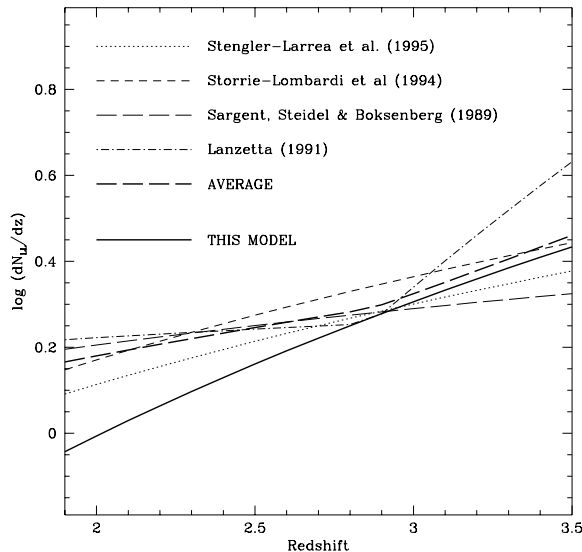


Figure 2. Number density of Lyman limit systems as observed by several authors (see labels) and produced by our method. The difference between our model and the average of the different observations is always less than 0.2dex in the redshift range of interest, and almost zero at $z \geq 2.8$.

$$\mathcal{L}(\tau_g) = \prod_{i=1}^{N_{\text{gal}}} \left(\frac{1}{N_{\text{sim}}} \sum_{j=1}^{N_{\text{sim}}} \frac{\exp \left[-\frac{(f_{\text{obs}}^{(i)} - f_{\text{sim}}^{(i,j)}(\tau_g))^2}{2\sigma_{\text{obs}}^{(i)2}} \right]}{\sqrt{2\pi\sigma_{\text{obs}}^{(i)2}} \right)}, \quad (3)$$

where the product extends over the N_{gal} galaxies of the sample and where the sum extends over the N_{sim} simulations of the analysis. We find that $N_{\text{sim}} = 100$ is enough to represent the variation of intervening Lyman series and Lyman limit absorption.

4 RESULTS AND DISCUSSION

Figure 3 shows results of the method described in § 3 applied to five examples of the galaxies. The examples are chosen to span a range in spectral type, redshift, and luminosity. For clarity, only 10 of the 100 realizations are presented for each galaxy. It is obvious from inspection of Figure 3 that in many cases (especially at the lowest redshifts) the fluxes observed through the F300W filter are less than the fluxes expected, if the galaxies were completely transparent to ionizing photons. This trend is also present in the other galaxies of the sample. Our quantitative maximum-likelihood analysis of this trend across the entire sample of galaxies establishes a lower limit to the optical depth at the Lyman limit or an upper limit to the escape fraction for these galaxies. In this section, we discuss these limits.

4.1 Galaxy Escape Fraction

Figure 4 and Table 2 show results of the method described in § 3 applied to the data described in § 2. The first panel of Figure 4 shows the relative likelihood as a function of $\log(\tau_g)$

determined from the entire sample of galaxies. The best-fit value of the galaxy Lyman-limit optical depth determined from the entire sample of galaxies is

$$\tau_g = 5.2_{-0.8}^{+1.4}, \quad (4)$$

and the corresponding best-fit value of the galaxy escape fraction determined from the entire sample of galaxies is

$$f_{\text{esc}} = 0.008 \pm 0.006. \quad (5)$$

These results apply at the average redshift of the entire sample of galaxies, which is

$$\langle z \rangle = 2.77 \quad (6)$$

The 3σ upper limit to the galaxy escape fraction determined from the entire sample of galaxies is

$$f_{\text{esc}} < 0.039. \quad (7)$$

Apparently, our analysis rules out the possibility of a large galaxy escape fraction at high significance but cannot rule out (at the 3σ level) the possibility of a galaxy escape fraction identically equal to zero. Based on these results, we conclude that *galaxies of redshift $z \approx 3$ are highly opaque to ionising photons.*

4.2 Possible selection Effects

Results of our analysis are apparently at odds with results of Steidel et al. (2001) that galaxies of $\langle z \rangle \approx 3.4$ are not highly opaque to ionizing photons. These authors observed in the average spectrum of 29 galaxies a flux ratio $F_{9/15} = 0.056$. After correcting for the effects of the Lyman α forest absorption using a composite QSO spectrum at the same redshift, they found an intrinsic flux ratio of $F_{9/15} = 0.22 \pm 0.05$ —where the effects of intrinsic galactic absorption and attenuation by dust or gas have not been eliminated. The authors further incorporated to this measurement a plausible estimate of the flux discontinuity at the Lyman limit due to absorption in stellar atmospheres to derive an escape fraction $f_{\text{esc}} \gtrsim 0.10$.¹

Steidel and collaborators suggested that the high escape fraction found in their work might result from some selection bias of their galaxy sample. The galaxies incorporated into their analysis include only 29 of 875 galaxies for which they obtained spectroscopic observations with the Keck telescope, selected on the basis of quality of the observations at blue wavelengths. This selection condition quite naturally selects galaxies that are either very blue, very luminous, or both. QSOs are known to be transparent to ionizing photons at ultraviolet wavelengths (Zheng *et al.* 1997), so it is not unreasonable to speculate that very blue or very luminous (or both) galaxies might exhibit larger escape fractions than average galaxies. To examine this possibility, we repeated the analysis described in § 3 for various subsamples of the galaxy sample.

¹ Steidel and collaborators used a definition of f_{esc} which is different from the usual one—they normalised the escape fraction at 900 Å to the escape fraction at 1500 Å. They reported $f_{\text{esc}} \gtrsim 0.50$, which is converted here to the usual definition assuming the escape fraction at 1500 Å is $\approx 0.15 - 0.20$ as quoted by the authors.

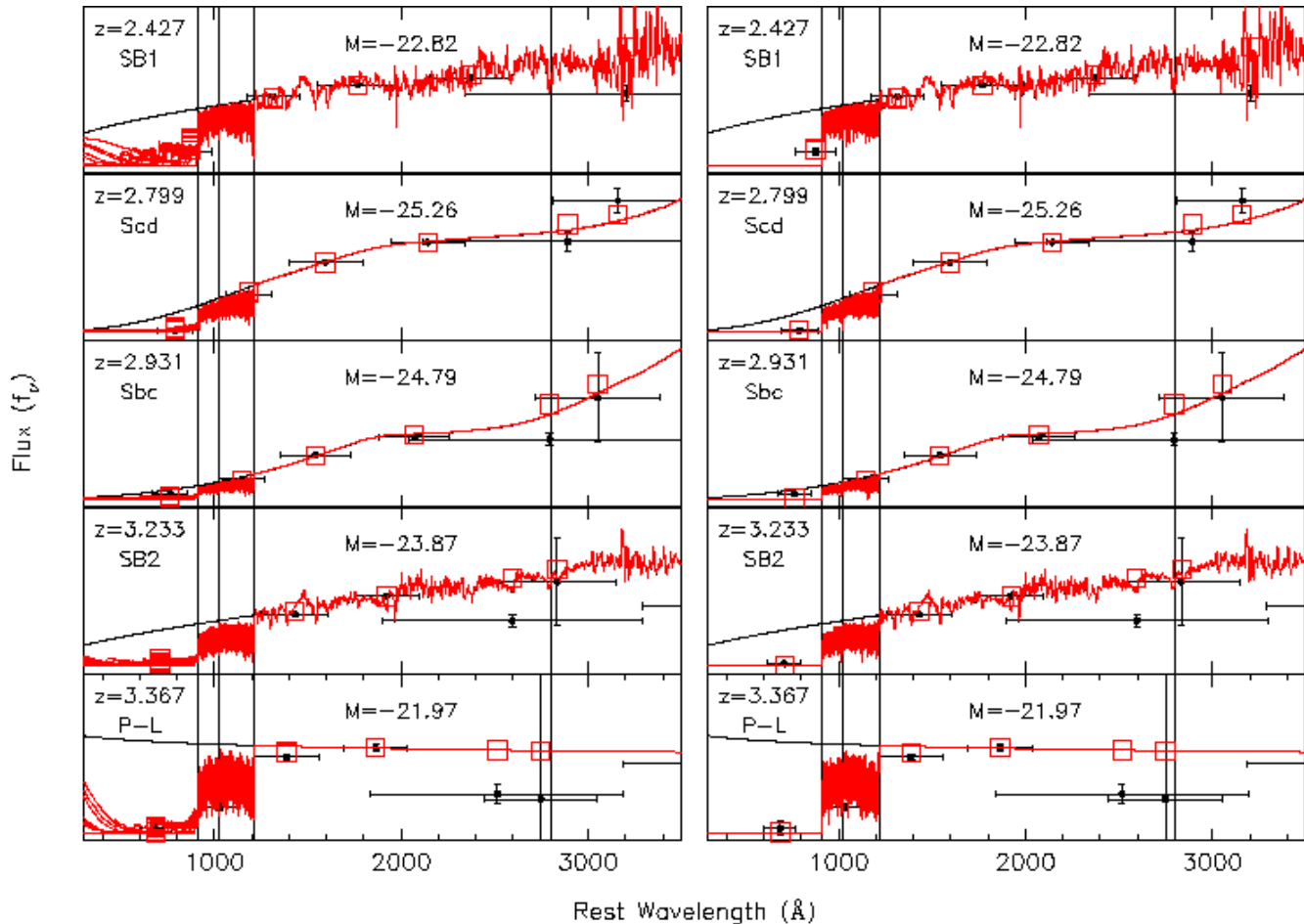


Figure 3. Photometry and model spectra (10 simulations each time) of a sample of galaxies with no intrinsic Lyman limit absorption ($\tau_g = 0$, left) and strong intrinsic absorption ($\tau_g = 10$, right). The vertical lines mark the positions of the Lyman limit, Lyman β and Lyman α lines, and $\lambda = 2800\text{\AA}$ in the rest frame. Circles with error bars show the photometric measurements. The squares show the photometry obtained from the fitted spectrum+HI absorption. The galaxies have been chosen to show the full range in redshift, type, and luminosity.

Color: First, we repeated the analysis for two subsamples of the galaxy sample divided according to color. Results are shown in the second panel of Figure 4 and the second group of entries in Table 2. Here “bluer” galaxies are galaxies best described by SB1 or power-law spectrophotometric templates and “redder” galaxies are galaxies best described by Scd, Irr, and SB2 spectrophotometric templates. Results obtained from both subsamples are consistent with each other and with results obtained from the entire sample of galaxies, although there is a (statistically insignificant) trend for the bluer galaxies to indicate a *smaller* galaxy escape fraction than is indicated by the redder galaxies. This result runs contrary to the idea described above.

Luminosity: Next, we repeated the analysis for two subsamples of the galaxy sample divided according to luminosity. Results are shown in the third panel of Figure 4 and the third group of entries in Table 2. Here “low-luminosity” galaxies are galaxies of absolute magnitude $AB > -23.75$ and “high-luminosity” galaxies are galaxies of absolute magnitude $AB < -23.75$. Results obtained from both subsamples are consistent with each other and with results obtained from the entire sample of galaxies, although there is a (statistically insignificant)

trend for the lower-luminosity galaxies to indicate a smaller galaxy escape fraction than is indicated by the higher-luminosity galaxies.

Redshift: Finally, we repeated the analysis for two subsamples of the galaxy sample divided according to redshift. Results are shown in the third panel of Figure 4 and the third group of entries in Table 2. Here “low-redshift” galaxies are galaxies of redshift $1.95 < z < 2.85$ and “high-redshift” galaxies are galaxies of redshift $2.85 < z < 3.50$. Results obtained from both subsamples are consistent with each other and with results obtained from the entire sample of galaxies, although there is a (statistically insignificant) trend for the lower-redshift galaxies to indicate a smaller galaxy escape fraction than is indicated by the higher-redshift galaxies. To some extent, this statistically insignificant difference could be due to the already mentioned relative lack of Lyman limit systems in our model at low redshift. Given that the results from the high-redshift sample (where our model reproduces exactly the observed number of Lyman limit systems) are not significantly different from the results obtained using the low redshift sample, we infer that the difference in the model does not induce a large change.

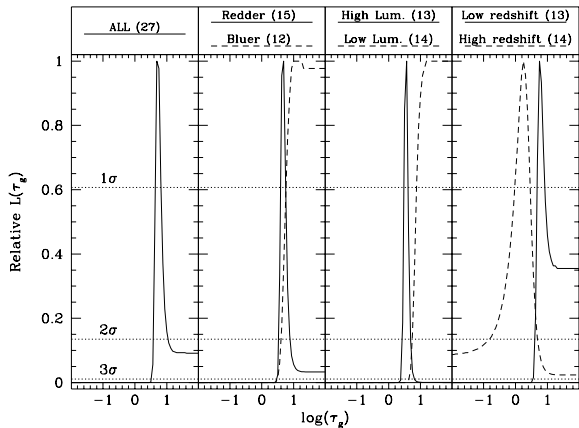


Figure 4. Relative likelihoods of the value of τ_g for the complete sample (left panel). The other panels show the results for different subsamples, broken according to (left to right) type, redshift, and luminosity. In all panels the horizontal lines correspond to statistical 1, 2, and 3 σ confidence intervals.

It should be remarked that *none of the subsamples analysed is different from the values given by the complete sample at the 3σ level*. Neither are any of the subsamples incompatible with their complementary subsamples at the same level. With this in mind, it is nevertheless interesting that the apparent effects of luminosity and ultraviolet blueness on f_{esc} seem to pull in opposite directions, suggesting that the higher escape fraction reported by Steidel and collaborators is unlikely due to selection effects.

4.3 Systematic uncertainties

All the confidence limits reported above refer only to the statistical properties of the sample of galaxies we are analysing. It is very likely that the method we are using to analyse the data may introduce errors of a systematic nature, that could potentially be of the same order of the statistical ones. We have performed some checks in order to estimate which could be the contribution from several sources of uncertainty.

4.3.1 Uncertainties induced by the Lyman α forest model

As was shown in §3 above, our Lyman α forest model has been checked against the observed properties, and agrees with them within observational limits. In order to estimate the uncertainty in f_{esc} that could originate from the uncertainties in the model, we have performed new measurements of f_{esc} using forest models that differ from our “standard” one by applying a 10% increase/decrease in the normalisation of the line density. We must remark that this 10% change does largely overestimate the possible uncertainties in our model—the models with 10% more or less lines represent bad fits to the observed forest properties.

As expected, an increase in the forest density implies an increase in the measured value of the escape fraction: more of the UV photons can escape each galaxy while keeping the observed photometric properties, as their mean free path is reduced by the increased density of absorbers. *Mutatis mutandis*, when the forest density is reduced, the value of

f_{esc} moves down. The change is, however, small: at the 3σ confidence level, the original limit ($f_{\text{esc}} < 0.039$) becomes $f_{\text{esc}} < 0.030$ ($f_{\text{esc}} < 0.046$) when the line density is decreased (increased) by 10%.

Another potential problem in our forest model could be the lack of clustering in our simulations, as opposed to what is shown by the observations. Our measurement is not affected by the small-scale clustering that has been observed in the Lyman α forest lines (Fernández-Soto *et al.* 1996) because we are integrating over much larger scales. Of potential importance is the observed clustering of high-column density absorbers (Sargent, Boksenberg & Steidel 1988). It is difficult to quantify its effect, but we expect it should be diluted by the size of our sample, and estimate that it produces a smaller variance than the one induced by the $\pm 10\%$ change in the number of lines presented above.

4.3.2 Uncertainties induced by the choice of the spectral templates

In the case of some of the galaxies, the photometric data available could allow for the assignment of two different fiducial spectral templates with similar goodness-of-fit values. The choice of one of them over the other (which we perform algorithmically via the minimum chi-squared criterium) could produce an extra uncertainty in the measurement of f_{esc} . The same effect can be produced if our selection of templates is not dense enough to cover the possible UV shapes, or if the photometric uncertainties are too big.

We have evaluated the uncertainty induced by this effect by performing the following exercise: we have forced all spectral templates to be one step bluer (always along the sequence formed by Ell, Sbc, Scd, Irr, SB2, SB1) than the one which is the best-fit choice³, and repeated the analysis. This does in fact result in very bad fits for many of the galaxies, and must thus be considered a *very large overestimate* of the possible uncertainties. Under this scenario, with the galaxies emitting far more ionising photons than what is indicated by their actual UV continua, the escape fraction diminishes to very low values: $f_{\text{esc}} < 0.016$ at the 3σ level.

We have also performed the opposite exercise, forcing all galaxies to be one step redder than their best-fit template⁴. Under this assumption the galaxies emit far less ionising photons than what their UV continua actually suggests, and this results in an increase in the acceptable escape fraction, which reaches $f_{\text{esc}} = 0.065$, with a 3σ upper limit $f_{\text{esc}} < 0.156$.

As we explained before, these limits must be taken as *very large overestimates* of the possible systematic effects induced by our spectroscopic templates, as we do not realistically expect to mistake all galaxies in the same direction. However, even under this extreme assumption, and incorporating also the effects described in §4.3.1, the upper limit to the measured escape fraction is still far below the values measured by Steidel *et al.* (2002).

³ Exception made of the ones that are already fitted by a SB1 template or a power-law

⁴ Exception made of those galaxies fitted by a power-law

Table 2. Measurements of f_{esc} obtained via the maximum likelihood method described in the text. The different subsamples used in the analysis are listed, together with the results and *statistical* confidence intervals associated to each one.

Sample	N ²	f_{esc}	1 σ Interval	2 σ Interval	3 σ Interval
All	27	0.008	(0.001–0.013)	(0.000–0.023)	(0.000–0.039)
Redder	15	0.008	(0.004–0.020)	(0.000–0.036)	(0.000–0.054)
Bluer	12	0.000	(0.000–0.003)	(0.000–0.018)	(0.000–0.047)
High Luminosity	13	0.026	(0.017–0.050)	(0.008–0.072)	(0.002–0.093)
Low luminosity	14	0.000	(0.000–0.001)	(0.000–0.004)	(0.000–0.013)
Low redshift	13	0.004	(0.000–0.008)	(0.000–0.018)	(0.000–0.030)
High redshift	14	0.169	(0.056–0.389)	(0.008–0.857)	(0.000–1.000)

5 CONCLUSIONS

We have presented a new method to measure the escape fraction of ionising photons from galaxies at $z \approx 3$. Our method provides a cleaner measurement compared to the classical spectroscopic technique because the problem of the sky subtraction is reduced almost to insignificance and we can use a wider bandpass.

The value we obtain ($f_{\text{esc}} = 0.008$, with $f_{\text{esc}} < 0.039$ at a 3σ confidence level) is in agreement with most previous measurements of the escape fraction of ionising photons at high and low redshift, being more stringent than most previous upper limits. It is largely in contradiction with the value presented by Steidel *et al.* (2001) for high-redshift galaxies⁵. We have studied possible selection effects that could cause this apparent difference and conclude that, *within the limits set by the size of our sample*, they cannot explain the large discordance between our results. Neither can the difference be explained by possible systematic effects induced by our method, as we also have shown. A (very conservative) estimate of the confidence limits when all systematic effects are included leads to a 3σ upper limit to the escape fraction that cannot be higher than $f_{\text{esc}} \lesssim 0.15$.

If the escape fraction of ionising photons reported here represents the general situation at high redshift, then normal galaxies cannot be responsible for any significant fraction of the high-redshift ionising background. On the other hand, if the proximity effect measurements of the background flux are confirmed, then the problem persists to find the objects responsible for the ionisation state of the high-redshift universe. Deep, narrow-band imaging of local and high-redshift galaxies at wavelengths slightly above and below their intrinsic Lyman limits could settle this argument. Such imaging campaigns would be less expensive, in terms of observing time, than the spectroscopic observations done to date.

6 ACKNOWLEDGMENTS

We thank our referee, Emanuele Giallongo, for his useful comments that have improved the clarity of our paper. AFS

gratefully acknowledges support by a Marie Curie Fellowship of the European Community programme “*Improving the human research potential and the socio-economic knowledge base*” under contracts number MCFI-1999-00494 and MCFI-2002-00472. HWC acknowledges the hospitality of the Osservatorio di Brera-Merate where this work was completed.

REFERENCES

- Bechtold, J., Green, R.F., Weymann, R.J., Schmidt, M., Estabrook, F.B., Sherman, R.D., Wahlquist, H.D., Heckman, T.M. 1984, ApJ, 281, 76
- Benítez N. 2000, ApJ, 536, 571
- Cohen J.G., Hogg D.W., Blandford R., Cowie L.L., Hu E.M., Songaila A., Shopbell P., Richberg K. 2000, ApJ, 538, 29 (C00)
- Dawson S., Stern D., Bunker A.J., Spinrad H., Dey A. 2001, AJ, 122, 598 (D01)
- Deharveng J.-M., Buat V., Le Brun V., Milliard B., Kunth D., Shull J.M., Gry C. 2001, A&A, 375, 805
- Ferguson, H.C. 2001, in Proc. ESO Symp. “Deep Fields”, ed. Cristiani, S., Renzini, A., & Williams, R.E. (Heidelberg: Springer) (also astro-ph/0101356)
- Fernández-Soto A., Barcons X., Carballo R., Webb J.K. 1995, MNRAS, 277, 235
- Fernández-Soto, A., Lanzetta, K.M., Barcons, X., Carswell, R.F., Webb, J.K., Yahil, A. ApJ, 1996, 460, L85
- Fernández-Soto, A., Lanzetta, K.M., Yahil, A. 1999, ApJ, 513, 34 (FLY99)
- Fernández-Soto, A., Lanzetta, K.M., Chen, H.-W., Pascarelle, S.M., Yahata, N. 2001, ApJS, 135, 41
- Giallongo E., Cristiani S. 1990, MNRAS, 247, 696
- Giallongo, E., Cristiani, S., D’Odorico, S., Fontana, A., Savaglio, S. 1996, ApJ, 466, 46
- Giallongo E., Cristiani S., D’Odorico S., Fontana A. 2002, ApJ, 568, L9
- Giroux M.L., Shapiro P.R. 1996, ApJS, 102, 191
- Hurwitz M., Jelinsky P., Dixon W.V.D. 1997, ApJ, 481, L31
- Kulkarni V.P., Fall S.M. 1993, ApJ, 413, L63
- Lanzetta K.M. 1991, ApJ, 375, L1
- Lanzetta K.M., Yahil A., Fernández-Soto A. 1996, Nature, 381, 759
- Leitherer C., Ferguson H.C., Heckman T.M., Lowenthal J.D. 1995, ApJ, 454, L19
- Liske J., Williger G.M. 2001, MNRAS, 328, 653
- Loeb, A., Eisenstein, D.J. 1995, ApJ, 448, 17
- Madau P., Shull J.M. 1996, ApJ, 457, 551
- Miralda-Escudé J., Ostriker J.P. 1990, ApJ, 350, 1

⁵ Steidel *et al.* (2001) remark that their results “should be treated as preliminary until high quality observations of individual galaxies exhibiting clear evidence for Lyman continuum photon leakage become available”

- O'Brien, P.T., Wilson, R., Gondhalekar, P.M. 1988, MNRAS, 233, 801
- Oke, J.B., Korycansky, D.G. 1982, ApJ, 255, 110
- Pascarella S.M., Lanzetta K.M., Chen H.-W., Webb J.K. 2001, ApJ, 560, 101
- Sargent, W.L.W., Boksenberg, A., Steidel, C.C. 1988, ApJS, 68, 539
- Sargent, W.L.W., Steidel, C.C., Boksenberg, A. 1989, ApJS, 69, 703
- Schneider, D.P., Schmidt, M., Gunn, J.E. 1989, AJ, 98, 1507
- Schneider, D.P., Schmidt, M., Gunn, J.E. 1991, AJ, 101, 2004
- Scott J., Bechtold J., Dobrzycki A., Kulkarni V.P. 2000, ApJS, 130, 67
- Steidel C.C., Pettini M., Adelberger K.L. 2001, ApJ, 546, 665
- Steidel, C.C., Sargent, W.L.W. 1987, ApJ, 313, 171
- Stengler-Larrea, E. *et al.* 1995, ApJ, 444, 64
- Storrie-Lombardi, L.J., McMahon, R.G., Irwin, M.J., Hazard, C. 1994, ApJ, 427, L13
- Yahata N., Lanzetta K.M., Chen H.-W., Fernández-Soto A., Pascarella S., Yahil A., Puetter R.C. 2000, ApJ, 538, 493 (Y00)
- Zheng W., Kriss G.A., Telfer R.C., Grimes J.P., Davidsen A.F. 1997, ApJ, 475, 469